

Electronic Supplementary Material (ESI) for Journal of Materials Chemistry A. This journal is © The Royal Society of Chemistry 2017

Supplementary Information

Defects Engineering of Highly Stable Lanthanide Metal-Organic Frameworks by Particle Modulation for Coating Catalysis

Yifa Chen^{1†}, Shenghan Zhang^{1†}, Fan Chen¹, Sijia Cao¹, Ya Cai¹, Siqing Li¹, Hongwei Ma¹, Xiaojie Ma¹, Pengfei Li^{1,2*}, Xianqiang Huang^{3*} and Bo Wang^{1*}

¹Beijing Key Laboratory of Photoelectronic/Electrophotonic Conversion Materials, Key Laboratory of Cluster Science, Ministry of Education, School of Chemistry, Beijing Institute of Technology, Beijing 100081, P. R. China.

*E-mail: bowang@bit.edu.cn

²Advanced Research Institute for Multidisciplinary Science, Beijing Institute of Technology, Beijing 100081, P. R. China.

*E-mail: lipengfei@bit.edu.cn

³Shandong Provincial Key Laboratory of Chemical Energy Storage and Novel Cell Technology, School of Chemistry & Chemical Engineering, Liaocheng University, Liaocheng, 252059, P. R. China.

*E-mail: hxqqxh2008@163.com

This PDF file includes:

Materials and Methods

Figure S1 to S23

Table S1

Table of Contents

- 1. Materials***
- 2. Characterization and instruments***
- 3. Synthesis of BIT-58, La-BTB, Ce-BTC, Eu-BTC, Dy-BTC and Ce-NDC***
- 4. Synthesis of BIT-58, La-BTB, Ce-BTC, Eu-BTC, Dy-BTC and Ce-NDC nanoparticles with the addition of 1-methylimidazole (1-mIM)***
- 5. Fabrication of nano-BIT-58 based film or coating through electrospinning***
- 6. Chemical stability tests of BIT-58 and nano-BIT-58***
- 7. Thermal stability tests of BIT-58 and nano-BIT-58***
- 8. NH₃-TPD tests of BIT-58 and nano-BIT-58***
- 9. Catalysis experiments of BIT-58, nano-BIT-58, nano-BIT-58/PAN based film and coating***
- 10. Supplementary information references***

1. Materials

Ce(NO₃)₃·6H₂O (Energy Chemical, 98%), La(NO₃)₃·6H₂O (Energy Chemical, 98%), 1,3,5-tris(4-carboxyphenyl)benzene (BTB, Beijing HWRK Chem Co., Ltd), trimesic acid (BTC, Energy Chemical, 98%), 1-methylimidazole, 2,4-dimethylpyrrole, 1,2-dimethylimidazole, pyrrole, pyridine, 2,6-lutidine, piperazine, 2-methylimidazole, imidazole, benzimidazole, benzoic acid, 4-fluorobenzoic acid, 2-fluorobenzoic acid, formic acid, acetic acid are all purchased from Energy Chemical with purity > 98%, polyacrylonitrile (PAN, M.W. 150,000, J&K), DMF (Sinopharm Chemical Reagent Co., Ltd), methanol (Sinopharm Chemical Reagent Co., Ltd), ethanol (Sinopharm Chemical Reagent Co., Ltd), benzaldehyde, 4-chlorobenzaldehyde, 4-bromobenzaldehyde, 4-methoxybenzaldehyde, 3,5-dimethoxybenzaldehyde, 1-naphthaldehyde, 9-anthraldehyde are all purchased from Aladdin with purity > 98%, malononitrile (Aladdin, 99%), 2-benzylidenemalononitrile (Aladdin, 99%), All the reagents used in this work were used as received without further purification.

2. Characterization and instruments

Field-emission scanning electron microscopy (FESEM, S-4800) was applied to investigate the morphology of the samples. The composition information was conducted by energy dispersive X-ray spectroscopy (EDS) at 20 keV on a TN5400EDS instrument. Transmission electron microscopy (TEM) was carried out by a JEOL JEM-1200EX Transmission electron microscope. Single-crystal X-ray diffraction data was conducted on a BrukerAXS CCD diffractometer equipped with a graphite-monochromated Mo-K α radiation ($\lambda = 0.71073 \text{ \AA}$) at 77 K. Powder X-ray

diffraction (PXRD) was performed on a MiniFlex 600 diffractometer with a Cu-K α X-ray radiation source ($\lambda = 0.154056$ nm). N₂ sorption tests were measured using a Bruker D8 Advance automatic volumetric gas adsorption analyser. Elemental analyses of Ce were determined by a PLASMA-SPEC (I) ICP atomic emission spectrometer. The C, H and N elemental analyses were conducted on Perkin-Elmer 240C elemental analyser. Thermogravimetric analysis (TGA) of samples was performed on a PerkinElmer STA6000 Simultaneous Thermal Analyzers using a constant heating rate of 10 °C min⁻¹ under N₂ atmosphere. X-ray photoelectron spectroscopy (XPS) measurements were performed on an American Thermo-VG Scientific ESCALAB 250XI XPS system with Al K α radiation as the exciting source. FT-IR spectra were recorded on Bruker (ALPHA) spectrometer. The GC analyses were performed on Shimadzu GC-2014C with a FID detector equipped with an HP-5ms capillary column. The GC mass spectra were recorded on Agilent 7890A-5975C at an ionization voltage of 1200 V. The pH value was measured by a Youke PHS-3E pH meter. High-frequency sonication was performed with an ultrasonic cell breaker (VOSHIN-1000W) with a frequency of 20 kHz. Tensile strength tests were measured with D&G DLL-5000 electronic tensile measure instrument. Processing of the filters was performed on a UCALERY SS-2534H electrospinning setup and a portable electrospinning (Bona-tech, Co., Ltd). The powder diffraction analysis was performed on TOPAS Professional 4.2 software. The background was modelled using a combination of a broad Gaussian function and a freely refining Chebyshev polynomial. Rietveld refinement was carried out from the

reported La-BTB structural model, with the position and isotropic displacement parameter of Ce atoms allowed to refine.^[1]

3. Synthesis of BIT-58, La-BTB, Ce-BTC, Eu-BTC, Dy-BTC and Ce-NDC

Synthesis of BIT-58:

Ce(NO₃)₃·6H₂O (138.6 mg, 0.320 mmol) was dissolved in 16 mL DMF/MeOH/H₂O (6 : 6 : 1) mixed solution with ultrasound for about 5 min in a 25 mL flask. 1,3,5-tris(4-carboxyphenyl)benzene (BTB, 48.0 mg, 0.0816 mmol) was added to the clear solution with ultrasound for about 1 min. The flask was tightly capped and heated in an oven at 85 °C under static conditions. After 24 h, the flask was cooled to room temperature in 2 h and light brown bulk crystals were obtained. The obtained crystals were washed with DMF and methanol each for 3 times. Yield: 54%. Anal. Calcd. for evacuated sample (C₂₇H₁₅CeO₆)·3.71H₂O·1.16DMF: Ce, 19.25, C, 50.34, H, 3.91. Found: Ce, 19.24, C, 50.32; H, 4.20. IR spectrum, ν (cm⁻¹): 1651 (s), 1610 (m), 1580 (s), 1520 (s), 1506 (s), 1407 (s), 1384 (s), 1248 (m), 1181 (m), 1144 (m), 1097 (m), 1016 (m), 851 (m), 815 (m), 778 (s), 701 (m), 666 (m), 469 (s).

Synthesis of La-BTB:

The synthesis of La-BTB follows the procedures reported in literature.^[2] La(NO₃)₃·6H₂O (138.6 mg, 0.320 mmol) was dissolved in 16 mL DMF/MeOH/H₂O (6 : 6 : 1) mixed solution with ultrasound for about 5 min in a 25 mL flask. 1,3,5-tris(4-carboxyphenyl)benzene (BTB, 48.0 mg, 0.0816 mmol) was added to the clear solution with ultrasound for about 1 min. The flask was tightly capped and heated in an oven at 85 °C under static conditions. After 24 h, the flask was cooled to

room temperature in 2 h and the colorless bulk crystals were obtained. The obtained crystals were washed with DMF and methanol each for 3 times.

Synthesis of Ce-BTC:

The synthesis of Ce-BTC follows the procedures reported in literature.^[3] Ce(NO₃)₃·6H₂O (434.1 mg, 1 mmol) and BTC (126.0 mg, 0.6 mmol) were dissolved in 6 mL DMF in a 10 mL Teflon-lined stainless steel autoclave. The autoclave was tightly capped and heated in an oven at 130 °C under static conditions. After 24 h, the autoclave was cooled to room temperature in 2 h and the colorless crystals were obtained. The obtained crystals were washed with DMF and ethanol each for 3 times.

Synthesis of Eu-BTC:

The synthesis of Eu-BTC follows the procedures reported in literature.^[4] Eu(NO₃)₃·6H₂O (33.1 mg, 0.074 mmol) and BTC (15.6 mg, 0.074 mmol) were dissolved in DMF (3 mL), ethanol (EtOH, 3 mL), and H₂O (2 mL) in a 10 mL Teflon-lined stainless steel autoclave. The autoclave was tightly capped and heated in an oven at 80 °C under static conditions. After 24 h, the autoclave was cooled to room temperature in 2 h and the colorless needle crystals were obtained. The obtained crystals were washed with DMF and ethanol each for 3 times.

Synthesis of Dy-BTC:

The synthesis of Dy-BTC follows the procedures reported in literature.^[4] Dy(NO₃)₃·6H₂O (33.1 mg, 0.074 mmol) and BTC (15.6 mg, 0.074 mmol) were dissolved in DMF (3 mL), ethanol (EtOH, 3 mL), and H₂O (2 mL) in a 10 mL Teflon-lined stainless steel autoclave. The autoclave was tightly capped and heated in

an oven at 80 °C under static conditions. After 24 h, the autoclave was cooled to room temperature in 2 h and the colorless needle crystals were obtained. The obtained crystals were washed with DMF and ethanol each for 3 times.

Synthesis of Ce-NDC:

The synthesis of Ce-NDC follows the modified procedures reported in literature.^[5] Ce(NO₃)₃·6H₂O (86.0 mg, 0.20 mmol) and 2,6-naphthalenedicarboxylic (NDC, 50.0 mg, 0.23 mmol) were dissolved in 10 mL DMF in a 25 mL flask. 0.01 mL NH₃·H₂O was added to the mixed solution with ultrasound for about 10 min. The flask was tightly capped and heated in an oven at 85 °C under static conditions. After 24 h, the flask was cooled to room temperature in 2 h and the colorless crystals were obtained. The obtained crystals were washed with DMF and ethanol each for 3 times.

4. Synthesis of BIT-58, La-BTB, Ce-BTC, Eu-BTC, Dy-BTC and Ce-NDC nanoparticles with the addition of 1-methylimidazole (1-mIM)

Ce(NO₃)₃·6H₂O (138.6 mg, 0.320 mmol) was dissolved in 16 mL DMF/MeOH/H₂O (6 : 6 : 1) mixed solution with ultrasound for about 5 min in a 25 mL flask. 1,3,5-tris(4-carboxyphenyl)benzene (BTB, 48.0 mg, 0.0816 mmol) was added to the clear solution with ultrasound for about 1 min. 1.2 mL 1-methylimidazole (1-mIM) was added to the mixed solution with ultrasound for about 10 min. The flask was tightly capped and heated in an oven at 85 °C under static conditions. After 24 h, the flask was cooled to room temperature in 2 h and light brown powder was obtained. The obtained powder was washed with DMF and methanol each for 3 times. Followed

the same procedures, different nano-BIT-58 with various amounts of 1-mIM added were synthesized and the morphologies were characterized (Figure S10).

Furthermore, the modulation effects of various modulators were investigated. Following the same procedures, various modulators (i.e. 2,4-dimethylpyrrole, 1,2-dimethylimidazole, pyrrole, pyridine, 2,6-lutidine, piperazine, 2-methylimidazole, imidazole, benzimidazole, benzoic acid, 4-fluorobenzoic acid, 2-fluorobenzoic acid, formic acid, acetic acid) with the same molar amounts were added to the same synthesis system as 1-mIM. After 24 h reaction the powder was collected and washed with DMF and ethanol (Figure S6-9).

Besides, we extended this protocol to La-BTB, Ce-BTC, Eu-BTC, Dy-BTC and Ce-NDC. 1.2, 1.6, 0.6, 0.6 and 0.75 mL 1-mIM were added into the precursor solution, respectively. Following the same procedures of La-BTB, Ce-BTC, Eu-BTC, Dy-BTC and Ce-NDC, nano-La-BTB, nano-Ce-BTC, nano-Eu-BTC, nano-Dy-BTC and nano-Ce-NDC particles were obtained, respectively (Figure S11 and S12).

5. Fabrication of nano-BIT-58 based film or coating through electrospinning

PAN solution:

0.4 g of PAN (M.W. 150,000) was added into 3.8 mL DMF and stirred for 12 h to form a homogeneous solution with a PAN concentration of 10 wt%.

Nano-BIT-58/PAN dispersion:

0.4 g of PAN was added into 1.6 mL DMF and stirred for 12 h. 0.933 g of nano-BIT-58 powder was dispersed in 3 mL DMF by high-frequency sonication (20 kHz) for 10 min. And then the nano-BIT-58 dispersion was mixed with PAN solution

and the mixture was stirred for 3 h to form a nano-BIT-58/PAN dispersion with a nano-BIT-58 loading of 70 wt%. As comparison, BIT-58/PAN dispersion was achieved following the same procedures for electrospinning.

Fabrication of nano-BIT-58 based film:

The nano-BIT-58/PAN (70 wt%) dispersion was loaded in a 5-ml syringe with 22-gauge needle tip. The dispersion was extruded out of the needle tip with a speed of 0.2 mm min⁻¹. A piece of aluminum foil was attached on the metal plate (the distance between needle and aluminum foil is 28 cm) to collect the electrospun nanofibers. The applied potential was 14 kV for electrospinning. After half an hour, a piece of film (~0.35 mm in thickness) with a diameter of 10 cm was obtained.

Fabrication of nano-BIT-58 based coating:

In 50 mL container, a portable electrospinning device with a 5 mL syringe which was loaded with nano-BIT-58/PAN (70 wt%) dispersion, was controlled by hand with a injection speed of about 1 cm h⁻¹. During the electrospinning procedures, the device was slowly moved in a clockwise direction around inner surface of the beaker to collect the electrospun nanofibers. After about 1 h, the beaker modified with nano-BIT-58/PAN coating (70 wt%) was achieved. Followed with the same procedures, container with various volumes (e.g. 30 mL) can also be modified.

Moreover, various substrates (i.e. aluminum foil, nickel foam, glass cloth, non-woven fabric, cardboard and plastic mesh) with size 4 × 4 cm² were used to collect the electrospun nanofibers. After about 30 min, the electrospun coatings on various substrates were achieved.

6. Chemical stability tests of BIT-58 and nano-BIT-58

The chemical stability tests of BIT-58 and nano-BIT-58 particles were performed through immersing the samples in various organic chemicals (e.g. aniline, chloroform, chlorobenzene, tetrahydrofuran, n-heptane) for 3 days, aqueous HCl solution (pH = 1), aqueous NaOH solution (pH = 12) for 24 hours, water (RT) for 10 days and boiling water (100 °C) for 3 days. All the samples after tests were collected by centrifugation and dried for further characterization (Figure S14).

7. Thermal stability tests of BIT-58 and nano-BIT-58

The thermal stability tests of BIT-58 and nano-BIT-58 particles in air or N₂ were tested by heating the samples from RT to target temperatures with a 5 °C min⁻¹ heating rate in a pipe furnace and kept at target temperatures for 30 min. All the samples after tests were collected and characterized by PXRD tests (Figure S3, S15).

8. NH₃-TPD tests of BIT-58 and nano-BIT-58

NH₃-TPD test was conducted by the pulse technique using a Micromeritics AutoChem II 2920 instrument using TCD detection (Figure S16). Before NH₃-TPD test, the sample was outgassed at 180 °C for 24 h. During the NH₃-TPD test, a sample of 100 mg was pretreated under a flow of helium (30 mL min⁻¹) at 300 °C for 3 h to remove water. Then the temperature was lowered to RT under a flow of He. The ammonia adsorption was performed at 100 °C for about 20 min. The NH₃-TPD data were collected from 50 °C to 500 °C at a heating rate of 10 °C min⁻¹ in a helium flow (Figure S16). The amount of physically adsorbed ammonia was collected to further reflect the defects of BIT-58 and nano-BIT-58.

9. Catalysis experiments of BIT-58, nano-BIT-58, nano-BIT-58/PAN based film and coating

Catalysis experiments of BIT-58 and nano-BIT-58:

Benzaldehyde (1 mmol, 0.1061 g), malononitrile (2 mmol, 0.1321 g) and catalyst sample (BIT-58 or nano-BIT-58, 0.05 mmol, 30 mg) was added in the reactor and heated at 60 °C for 6 h. For conversion rate experiments, small amount of the product was collected and detected every one hour. For the recycle experiments, the catalyst sample after every catalysis cycle was collected with centrifugation and washed with ethanol for several times and dried at 60 °C for 10 min.

Moreover, substrates with various molecule sizes (i.e. 4-chlorobenzaldehyde, 4-bromobenzaldehyde, 4-methoxybenzaldehyde, 3,5-dimethoxybenzaldehyde, 1-naphthaldehyde and 9-anthraldehyde) were added in the reactor with the same molar amount as benzaldehyde. After 6 h, the product was collected and detected (Table 1).

Catalysis experiments of nano-BIT-58/PAN based film:

Benzaldehyde (1 mmol, 0.1061 g), malononitrile (2 mmol, 0.1321 g) and nano-BIT-58/PAN based film (70 wt%, 0.0429g) were added in the reactor. The reactor was subsequently heated at 60 °C for 6 h. After catalysis, nano-BIT-58/PAN based film (70 wt%) can be recycled by simply pouring out the product solution and washed with ethanol. After dried at 60 °C for 10 min, the nano-BIT-58/PAN based film can be directly used in another cycle.

Catalysis experiments of nano-BIT-58/PAN based coating:

Benzaldehyde (2 mmol, 0.2122 g) and malononitrile (4 mmol, 0.2642 g) were added in 30 mL modified flask. The reactor was sealed and subsequently heated at 60 °C for 6 h. A high 95% conversion and 99% selectivity was achieved. After catalysis, the product can be ease of collection by pouring out without the need for separation of the catalyst. To ensure the data accuracy, the flask was washed with ethanol and dried at 60 °C for 10 min after each cycle and then tested its reusability. Recycle experiments were conducted by adding new substrate solution to this flask and this modified flask can be efficiently recycled.

Catalytic performance of the comparisons:

Benzaldehyde (1 mmol, 0.1061 g), malononitrile (2 mmol, 0.1321 g) and comparison (i.e. $\text{Ce}(\text{NO}_3)_3 \cdot 6\text{H}_2\text{O}$ (30 mg), BTB (30 mg) or PAN (9 mg)) were added into the reactor. The reactor was subsequently heated at 60 °C. After 6 h, the products in the reactor were collected by centrifugation and detected (Figure S21).

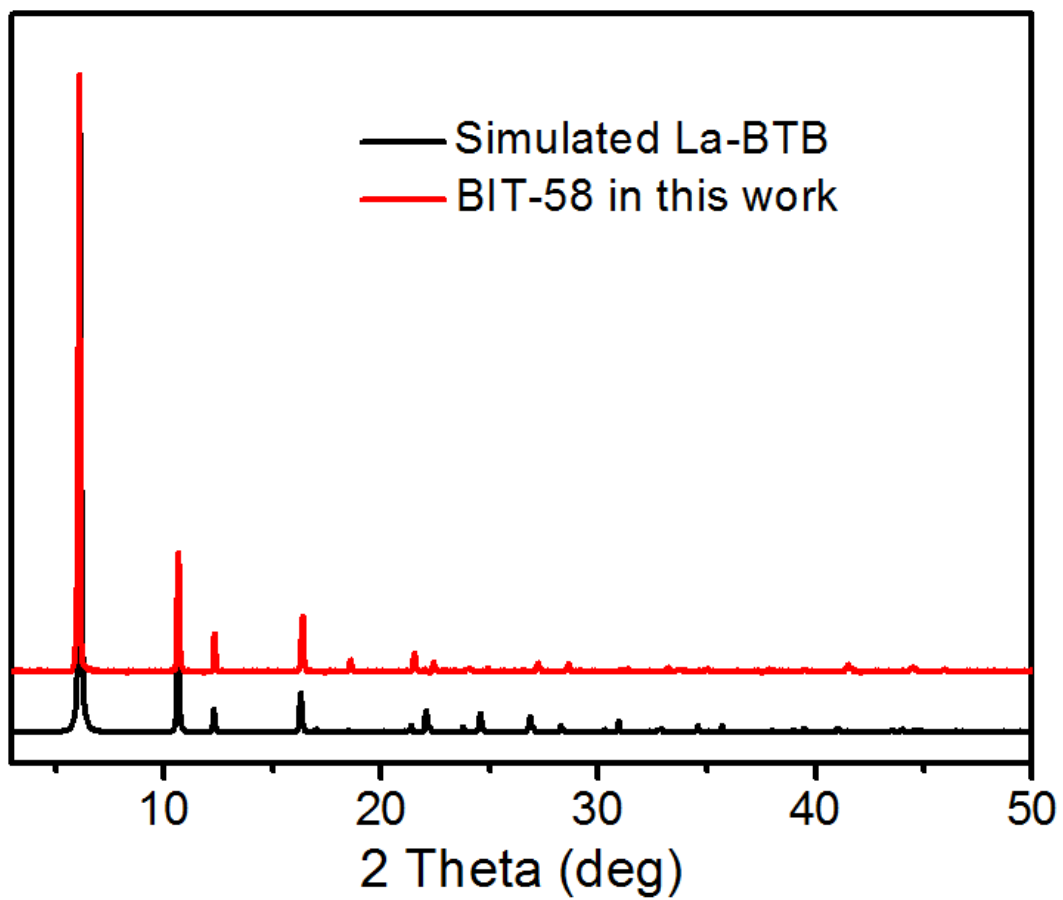


Figure S1. PXRD patterns of simulated La-BTB and BIT-58 in this work.^[2]

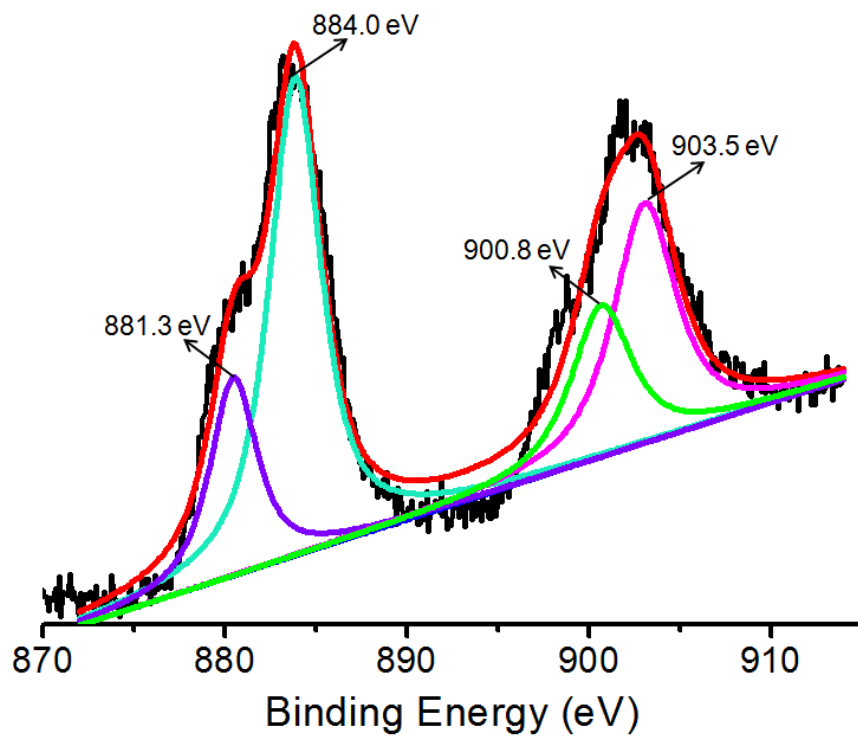


Figure S2. XPS Ce 3d photoemission spectra of BIT-58. Peaks at 881.3, 884.0, 900.8 and 903.5 eV are attributed the Ce^{III} in the BIT-58.^[6]

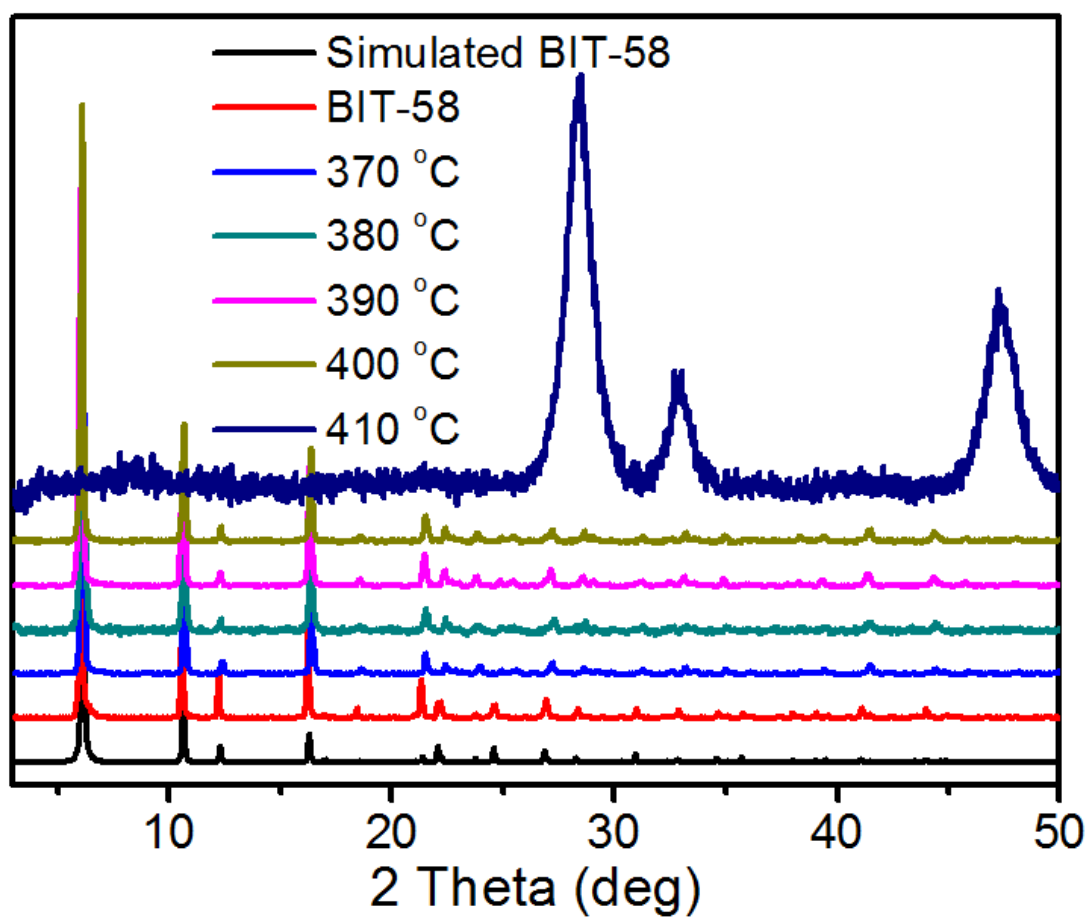


Figure S3. PXRD patterns of the thermal stability of BIT-58 in air.

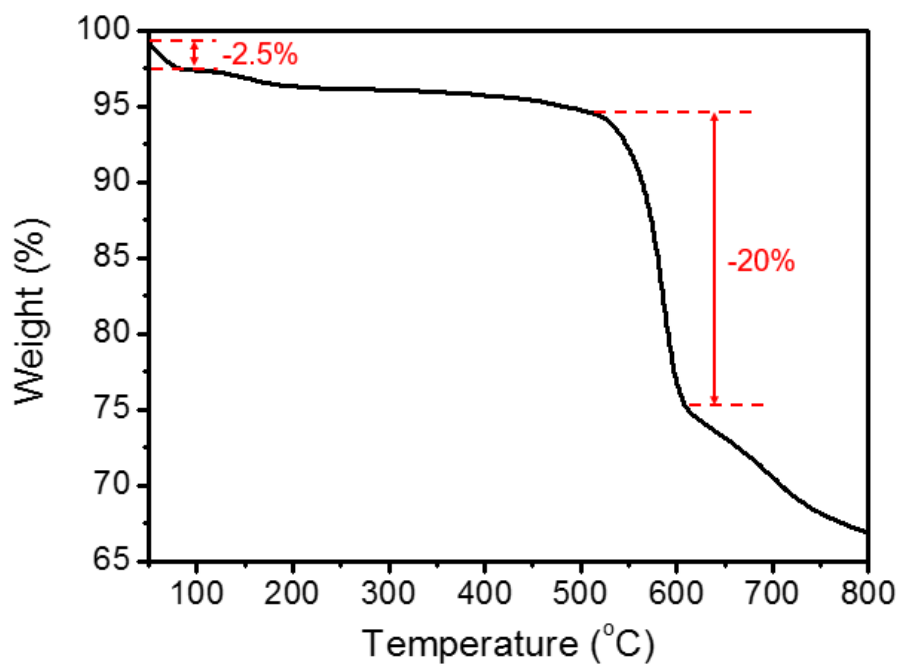


Figure S4. Thermogravimetric analysis (TGA) curve of BIT-58. 2.5% and 20% weight loss are attributed to the solvent evaporation and the decomposition of the structure, respectively.

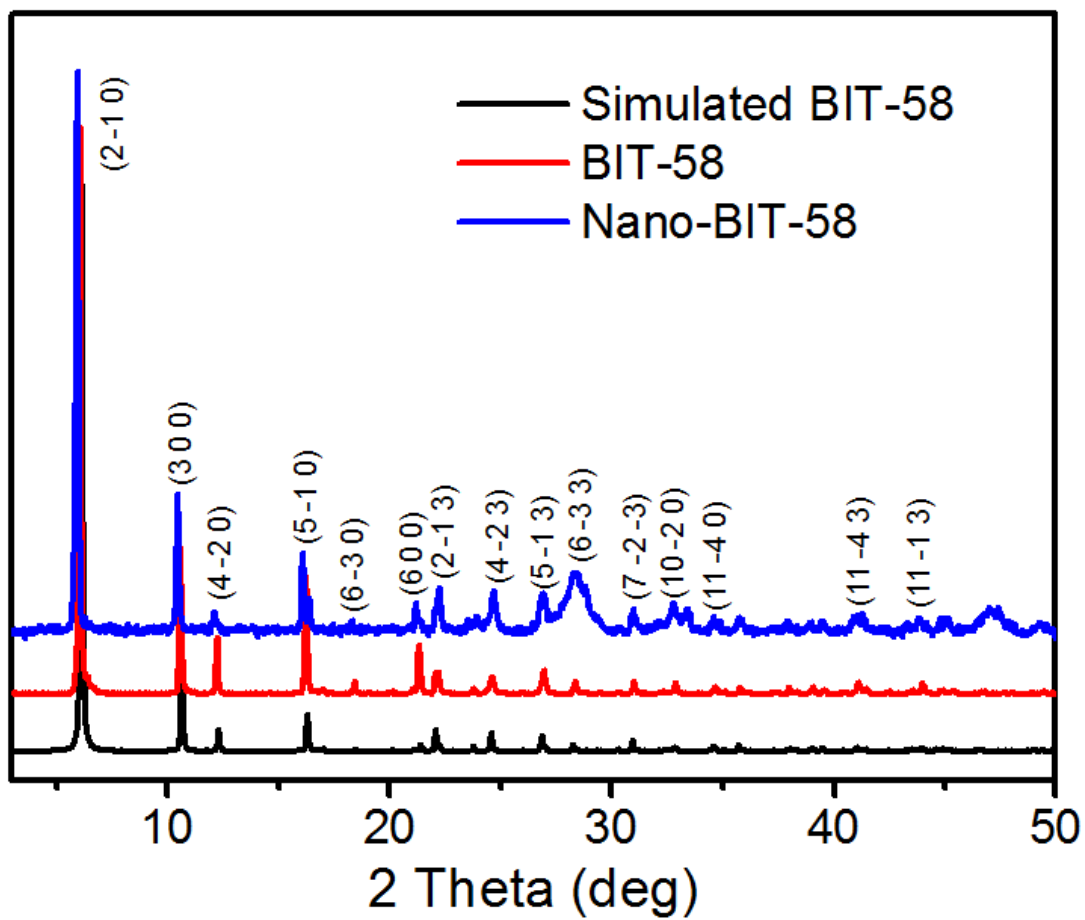


Figure S5. PXRD patterns of nano-BIT-58.

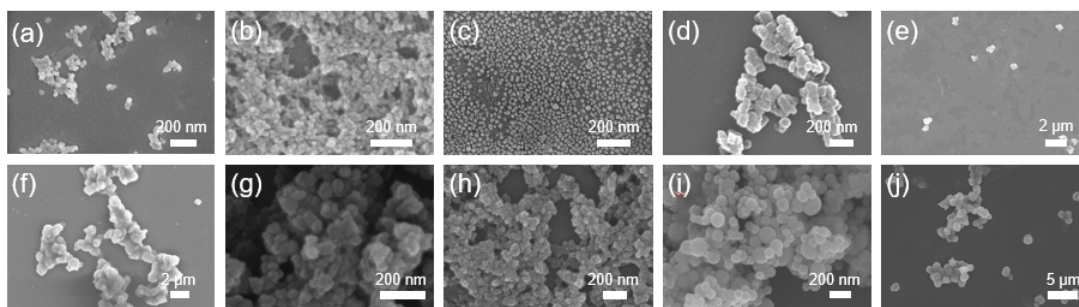


Figure S6. SEM images of BIT-58 nanoparticle treated with various N-coordinated modulators. a) 2,4-Dimethylpyrrole. b) 1,2-Dimethylimidazole. c) 1-Methylimidazole. d) Pyrrole. e) Pyridine. f) 2,6-Lutidine. g) Piperazine. h) 2-Methylimidazole. i) Imidazole. j) Benzimidazole. The syntheses of various BIT-58 nanoparticle were followed the same procedure and molar amount of 1-mIM. After 85 °C for 24 h, the obtained nano-BIT-58 were collected and washed with DMF and methanol for several times.

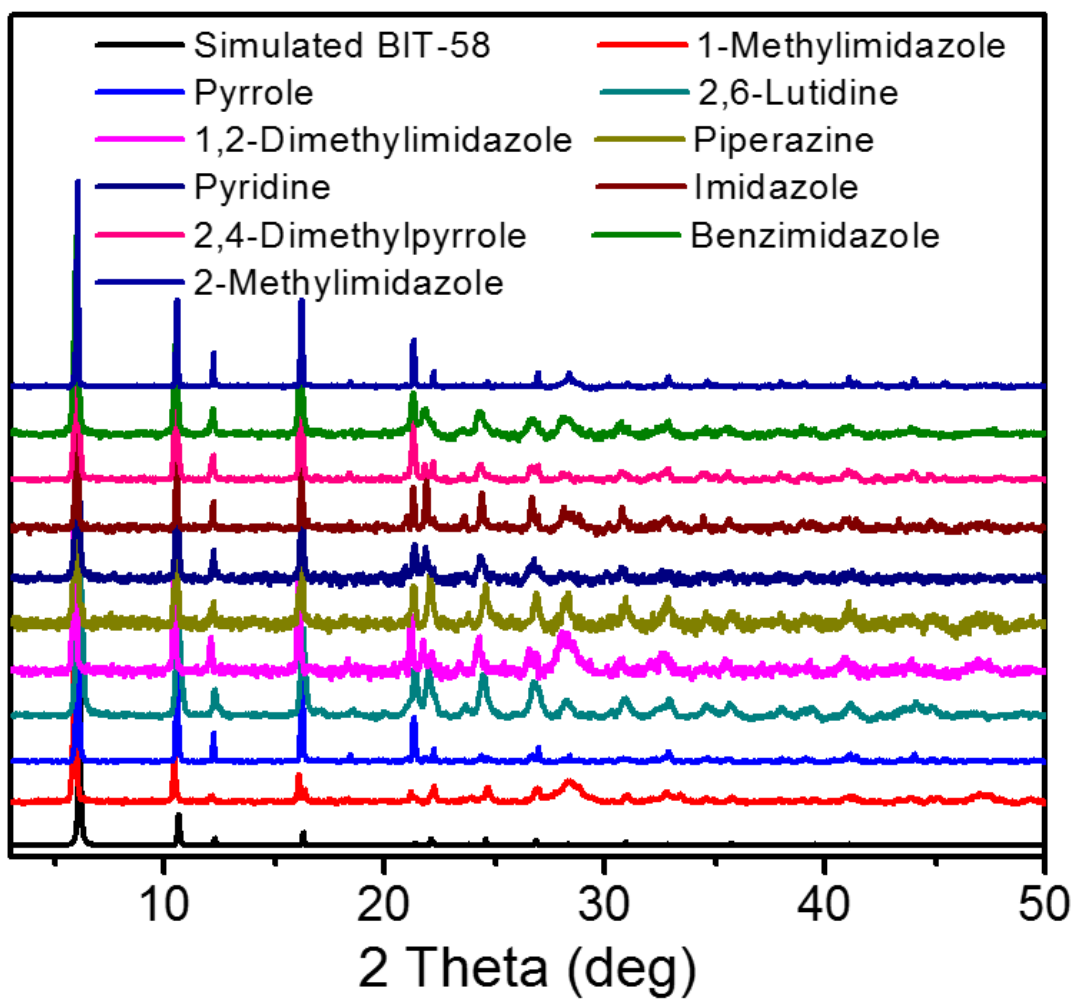


Figure S7. PXRD patterns of BIT-58 nanoparticle treated with various nitrogenous modulators.

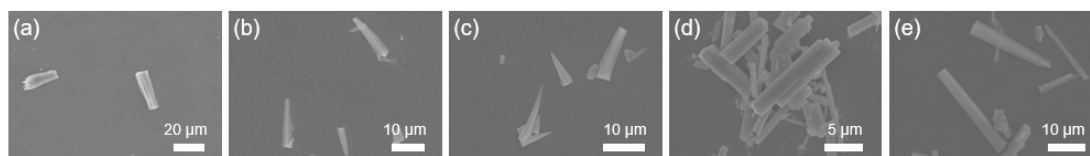


Figure S8. SEM images of BIT-58 synthesized with the addition of various carboxyl-containing modulators. a) Benzoic acid (about 30 μm). b) 4-Fluorobenzoic acid (about 20 μm). c) 2-Fluorobenzoic acid (about 15 μm). d) Formic acid (about 15 μm). e) Acetic acid (about 20 μm). The syntheses of various BIT-58 were followed the same procedure and molar amount of 1-mIM. After 85 $^{\circ}\text{C}$ for 24 h, the BIT-58 were collected and washed with DMF and methanol.

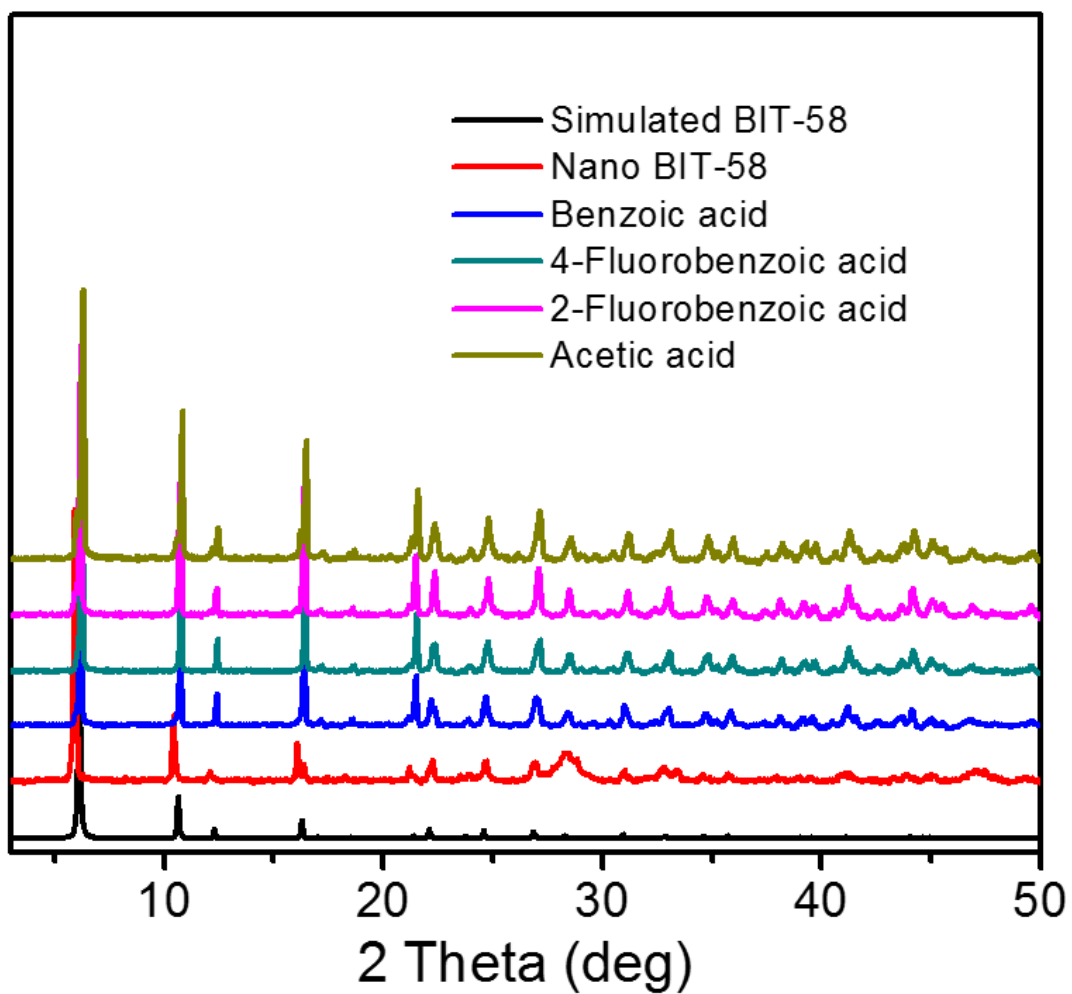
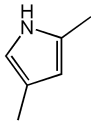
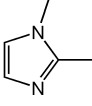
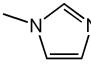
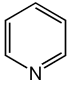
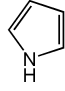
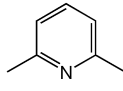
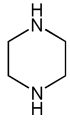
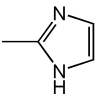
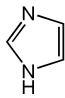
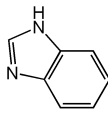


Figure S9. PXRD patterns of BIT-58 synthesized with the with the addition of various carboxyl-containing modulators.

Table S1. Polarizability and particle sizes of various modulators^{a)}.

Modulator (one coordination N site)	 2,4-Dimethyl- pyrrole	 1,2-Dimethyl- imidazole	 1-Methyl- imidazole	 Pyridine	 Pyrrole	 2,6-Lutidine
Polarizability (\AA^3) ^{b)}	12.02	11.76	10.01	9.65	8.20	13.47
Particle sizes ^{c)} (nm)	25 ± 8	28 ± 10	30 ± 12	90 ± 37	762 ± 61	1110 ± 201
Modulator (two coordination N sites)	 Piperazine	 2-Methylimidazole	 Imidazole	 Benzimidazole		
Polarizability (\AA^3)	9.96	9.35	7.44	14.51		
Particle sizes (nm)	35 ± 11	59 ± 16	105 ± 35	1363 ± 378		

a) Two groups of modulators are summarized in the Table S1, they are modulators with one and two coordination nitrogen sites. b) The data of calculated polarizability values of various modulators are obtained from a WINGCH Chemical Database. c) Particle sizes are calculated by a Nano Measure software (> 100 particles) and all the results are performed in triplicate.

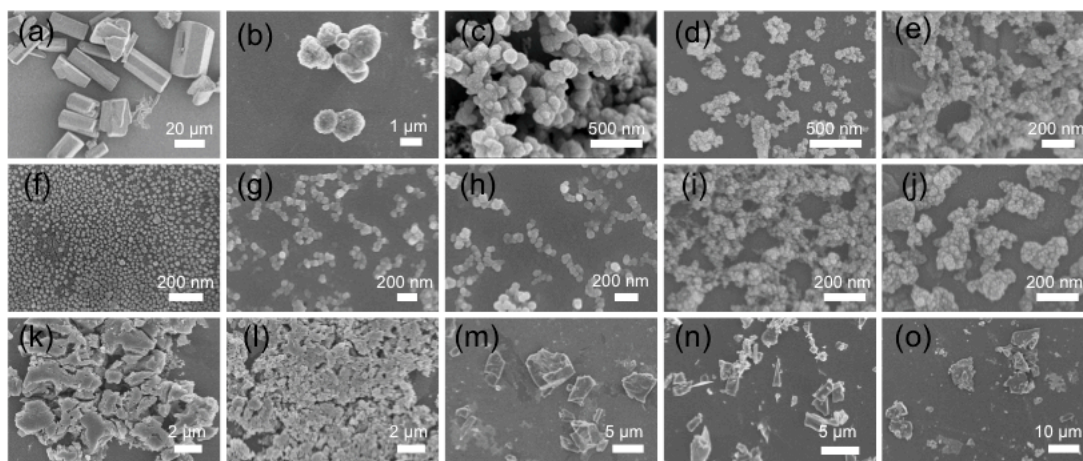


Figure S10. SEM images of nano-BIT-58 with various amounts of 1-mIM added. a) 0 mL. b) 0.4 mL. c) 0.6 mL. d) 0.8 mL. e) 1.0 mL. f) 1.2 mL. g) 1.4 mL. h) 1.6 mL. i) 1.8 mL. j) 2.0 mL. k) 3.0 mL. l) 6.0 mL. m) 7.0 mL. n) 8.0 mL. o) 9.0 mL.

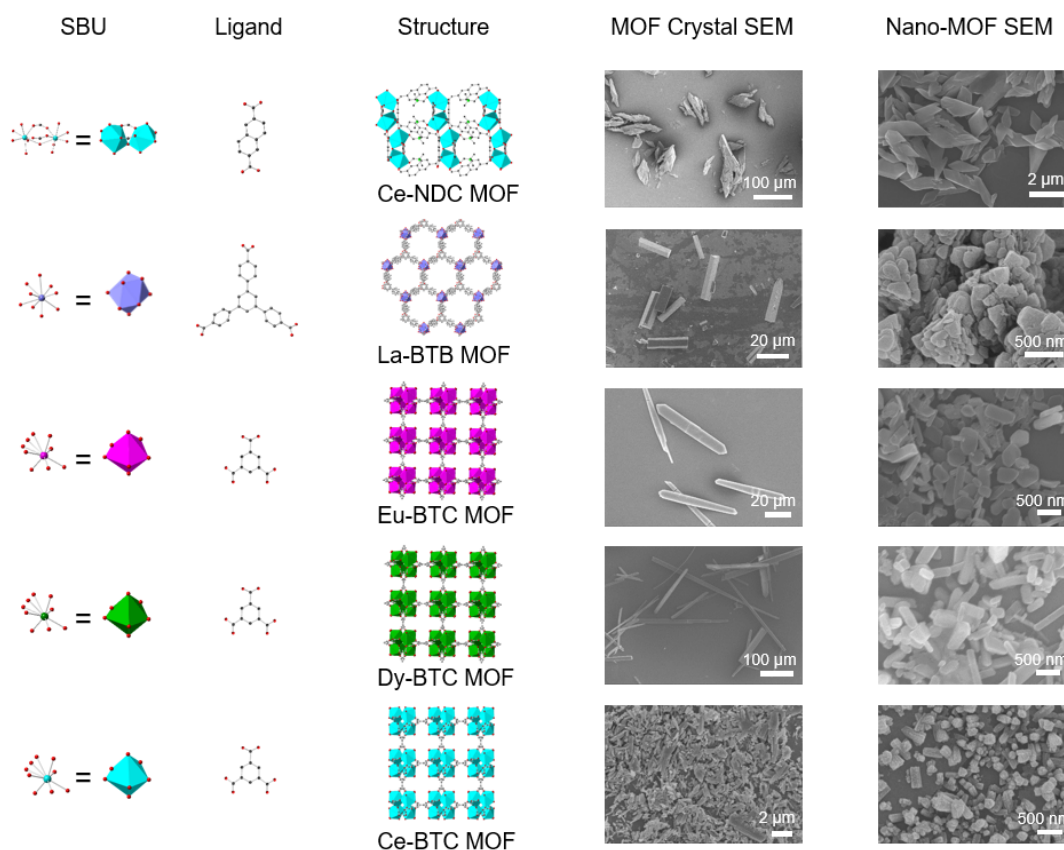


Figure S11. Structures and SEM images of Ce-NDC, La-BTB, Eu-BTC, Dy-BTC and Ce-BTC after particle modulation. The particle sizes of Ce-NDC and nano-Ce-NDC are about 80 μm and 1.5 μm , respectively. The particle sizes of the La-BTB and nano-La-BTB are about 30 μm and 200 nm, respectively. The particle sizes of Eu-BTC and nano-Eu-BTC are about 60 μm and 450 nm, respectively. The particle sizes of Dy-BTC and nano-Dy-BTC are about 190 μm and 600 nm, respectively. The particle sizes of Ce-BTC and nano-Ce-BTC are about 2 μm and 100 nm, respectively.

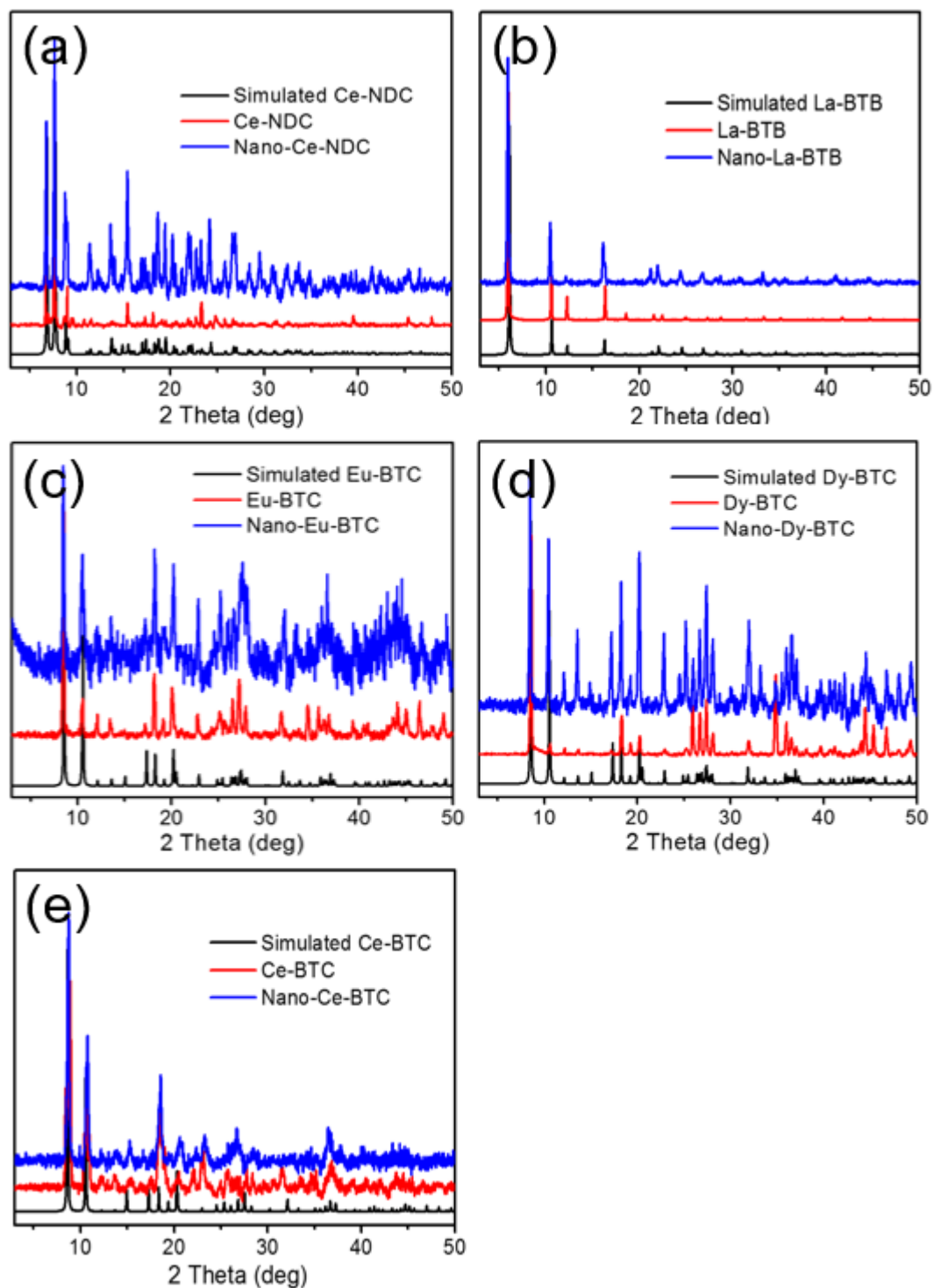


Figure S12. a) PXRD patterns of Ce-NDC and nano-Ce-NDC. b) PXRD patterns of La-BTB and nano-La-BTB. c) PXRD patterns of Eu-BTC and nano-Eu-BTC. d) PXRD patterns of Dy-BTC and nano-Dy-BTC. e) PXRD patterns of Ce-BTC and nano-Ce-BTC.

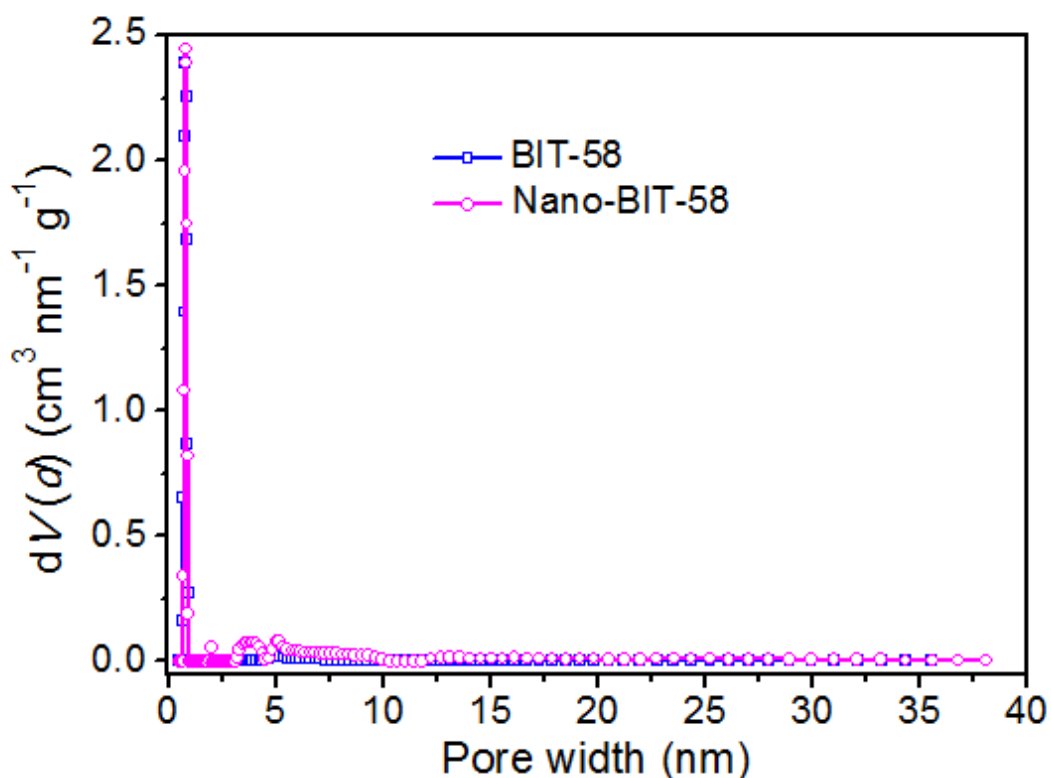


Figure S13. Pore size distributions of BIT-58 and nano-BIT-58, the pore size distribution model is N_2 at 77 K on carbon (silt/cylindr. pore, QSDFT adsorption model) with fitting error of 1.704% and 0.961% for BIT-58 and nano-BIT-58, respectively. Nano-BIT-58 possesses a total pore volume of $1.78 \text{ cm}^3 \text{ g}^{-1}$ (P/P_0 , 0.99) and $1.43 \text{ cm}^3 \text{ g}^{-1}$ (P/P_0 , 0.95, $< 20 \text{ nm}$), which is more than twice compared with BIT-58 ($0.82 \text{ cm}^3 \text{ g}^{-1}$, P/P_0 , 0.99 and $0.40 \text{ cm}^3 \text{ g}^{-1}$, P/P_0 , 0.95, $< 20 \text{ nm}$).

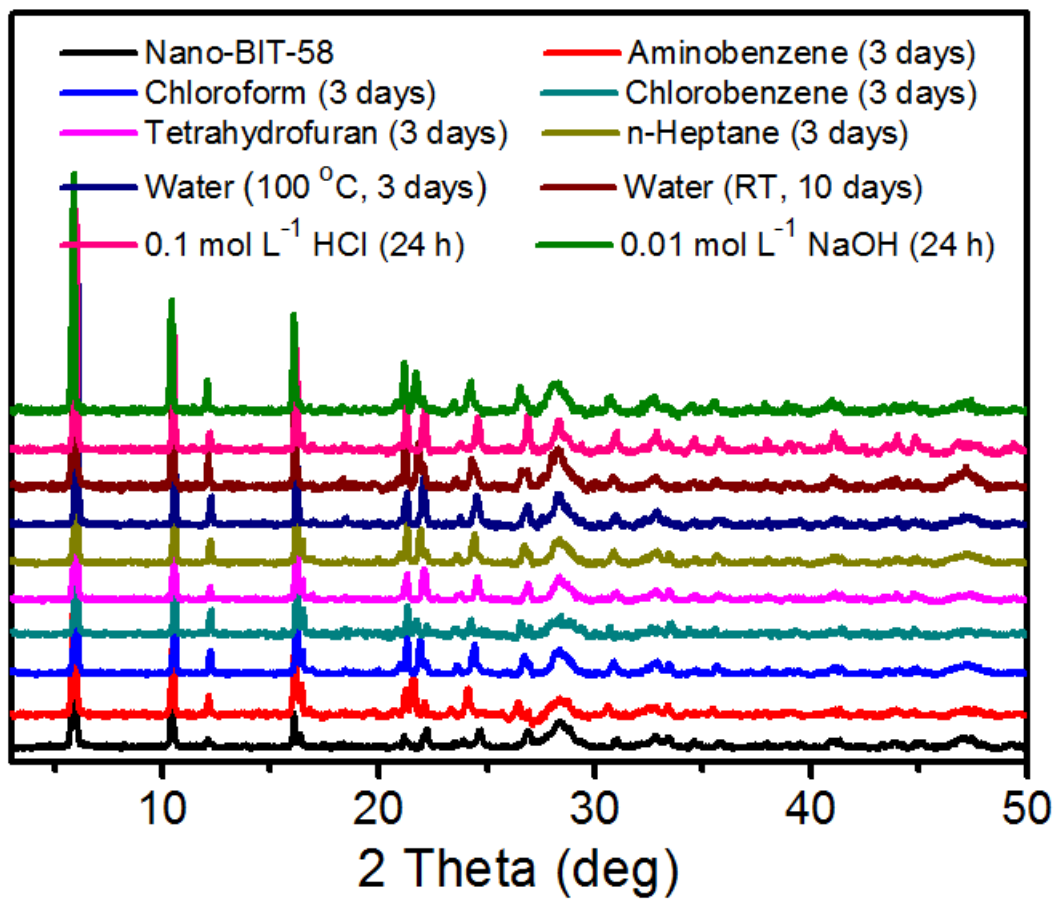


Figure S14. PXRD patterns of the chemical stability of nano-BIT-58.

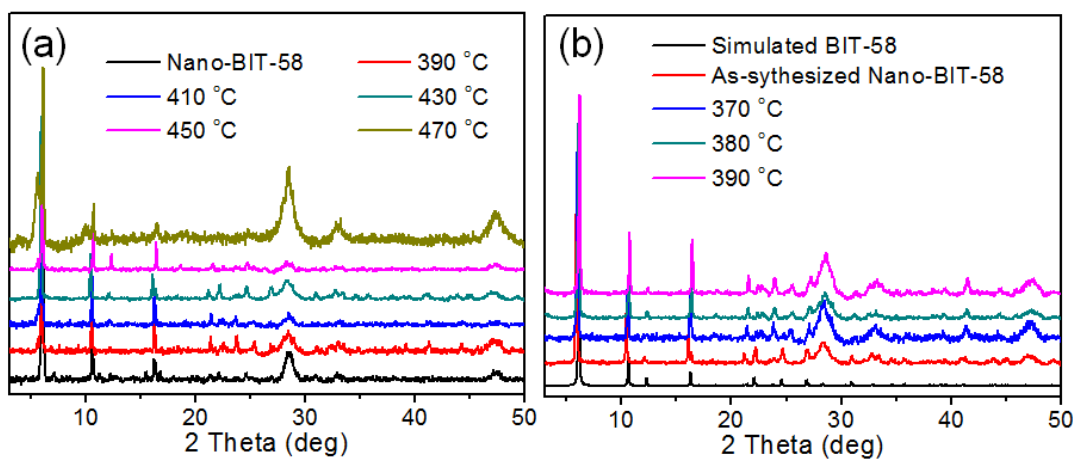


Figure S15. PXRD patterns of the thermal stability of nano-BIT-58 in N₂ and air. a) The thermal stability of nano-BIT-58 in N₂. b) The thermal stability of nano-BIT-58 in air.

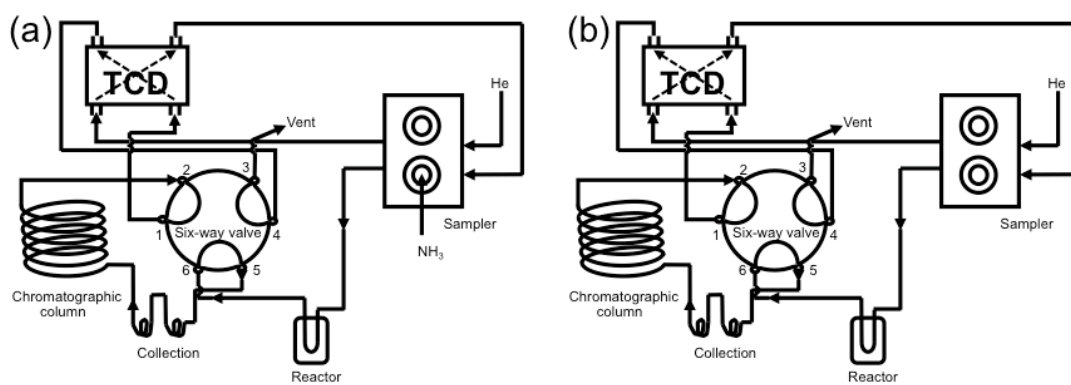


Figure S16. The schematic representation of the NH₃-TPD device. a) The schematic representation of adsorption device of NH₃-TPD. b) The schematic representation of desorption device of NH₃-TPD.

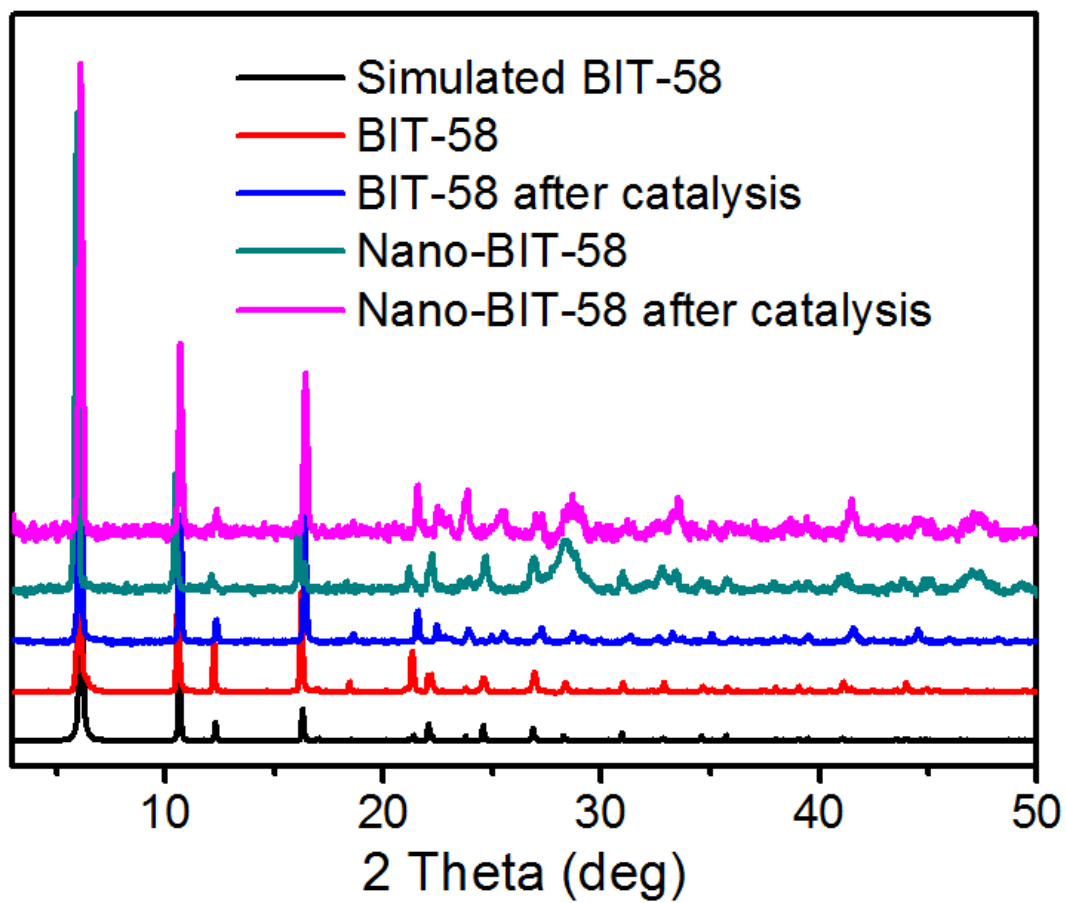


Figure S17. PXRD patterns of BIT-58 and nano-BIT-58 after catalysis.

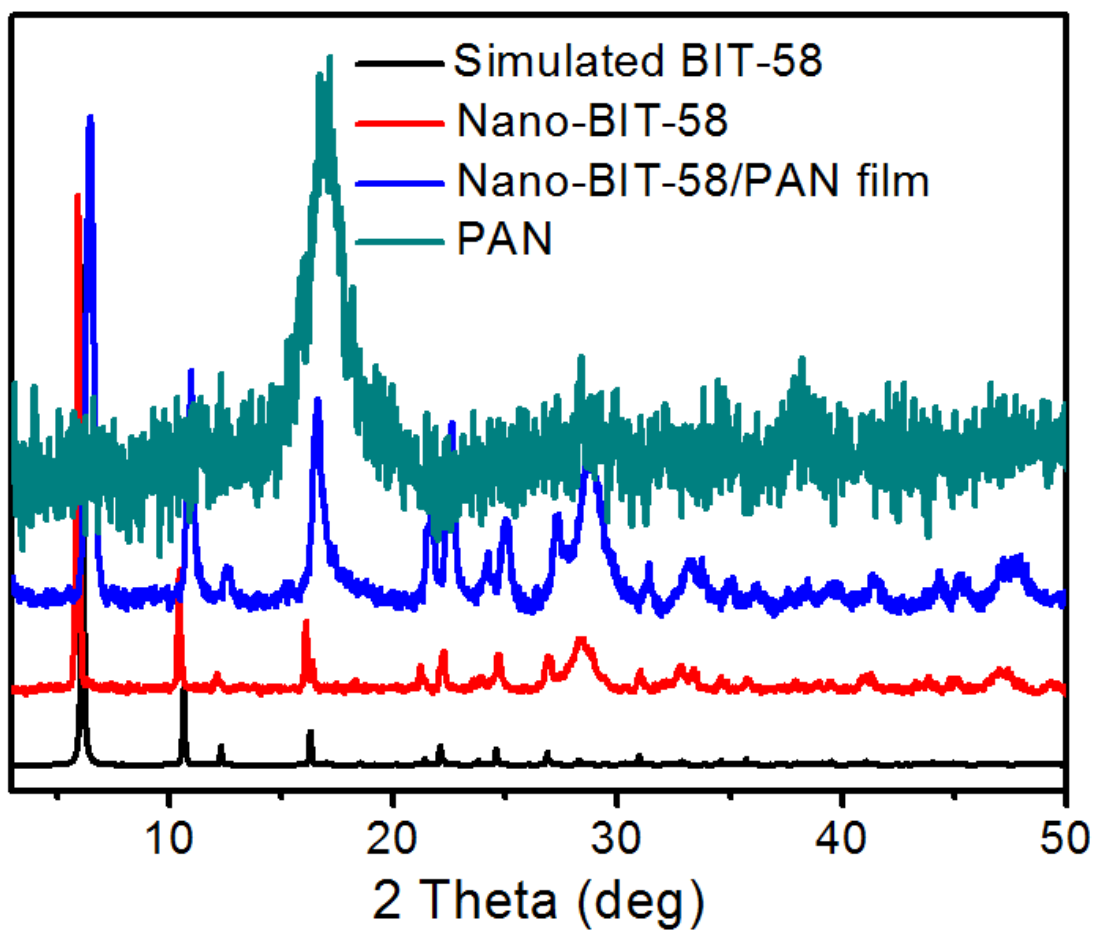


Figure S18. PXRD patterns of nano-BIT-58/PAN based film (70 wt%).

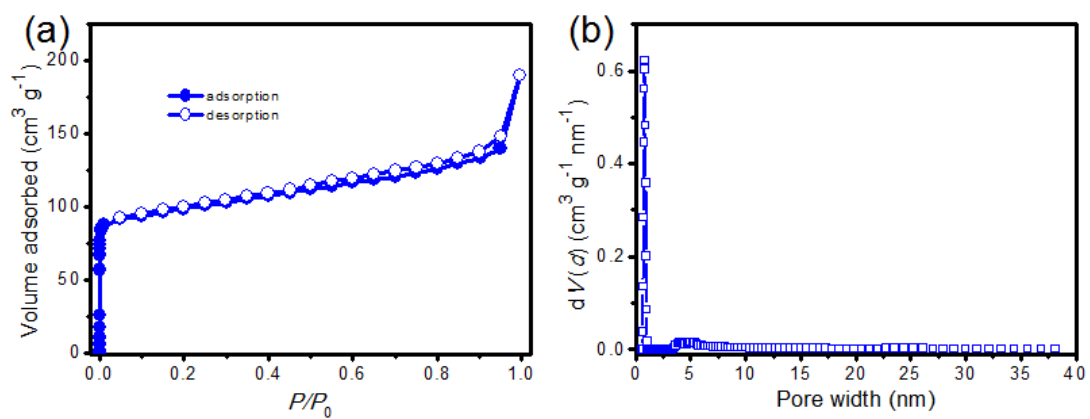


Figure S19. N₂ sorption test of nano-BIT-58/PAN based film (70 wt%). a) N₂ sorption curve of nano-BIT-58/PAN based film (70 wt%). b) Pore size distribution of nano-BIT-58/PAN based film (70 wt%).

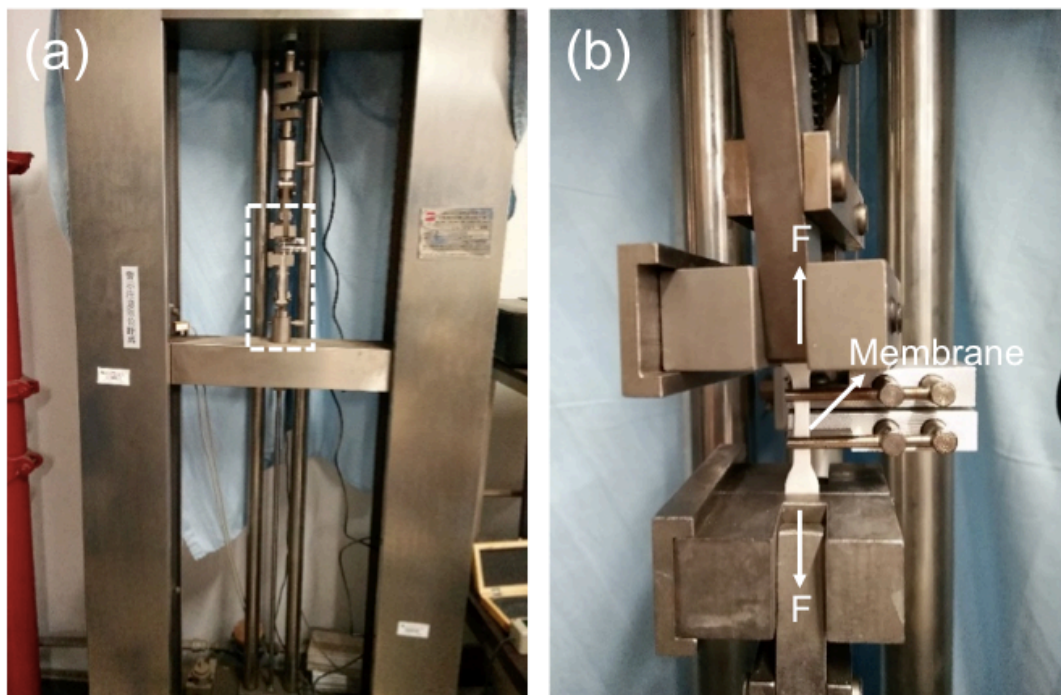


Figure S20. Photo images of nano-BIT-58 based film under tensile strength test. a) Photo image of tensile strength test device. b) The zoom-in image of the square box in a. Nano-BIT-58 based film during test. The tensile strength followed EN ISO527-1:1996 standard. A piece of nano-BIT-58 based film (0.35 mm in thickness, 2 cm in length and 4 mm in width) was placed in the mould and a force was triggered to drag the nano-BIT-58 based film in different directions. With the increase of force, the nano-BIT-58 based film was drawn longer and longer until it was broken. During this process, the data curve was recorded in a PC. Data reported in this work was the largest pressure when the nano-BIT-58 based film broke. The tensile strength values of nano-BIT-58 based film and nano-BIT-58 based film after catalysis are 0.05 and 0.08 MPa, respectively.

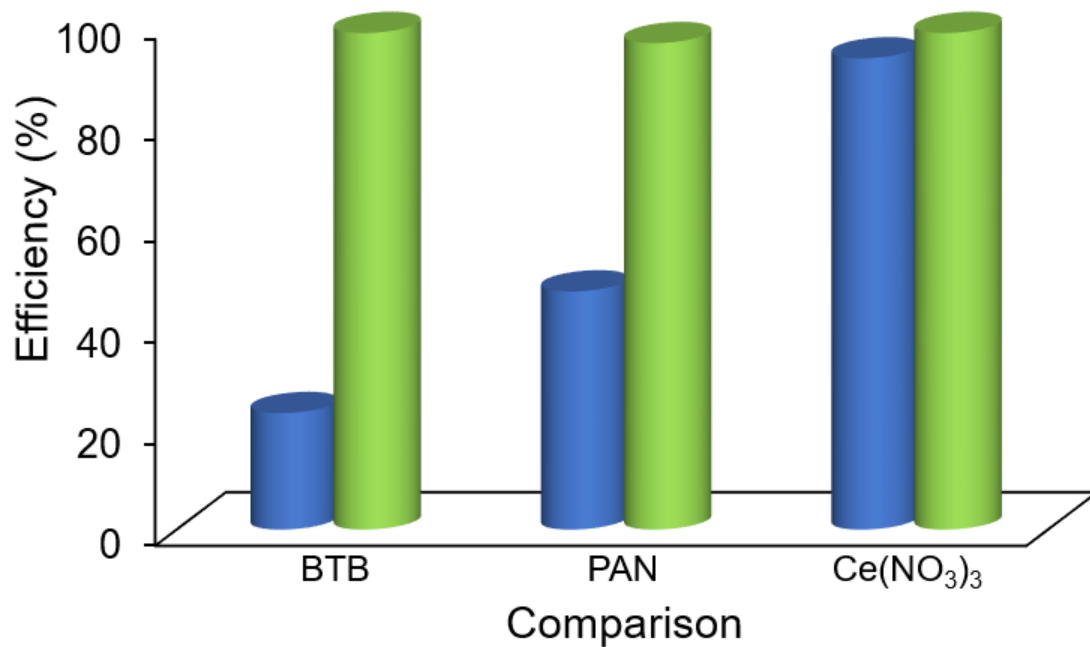


Figure S21. Catalytic efficiency of comparison (BTB, PAN, Ce(NO₃)₃·6H₂O). Blue, conversion; green, selectivity. After reacting at 60 °C for 6 h, BTB, PAN and Ce(NO₃)₃·6H₂O reach a 23%, 47%, and 96% conversion, respectively.

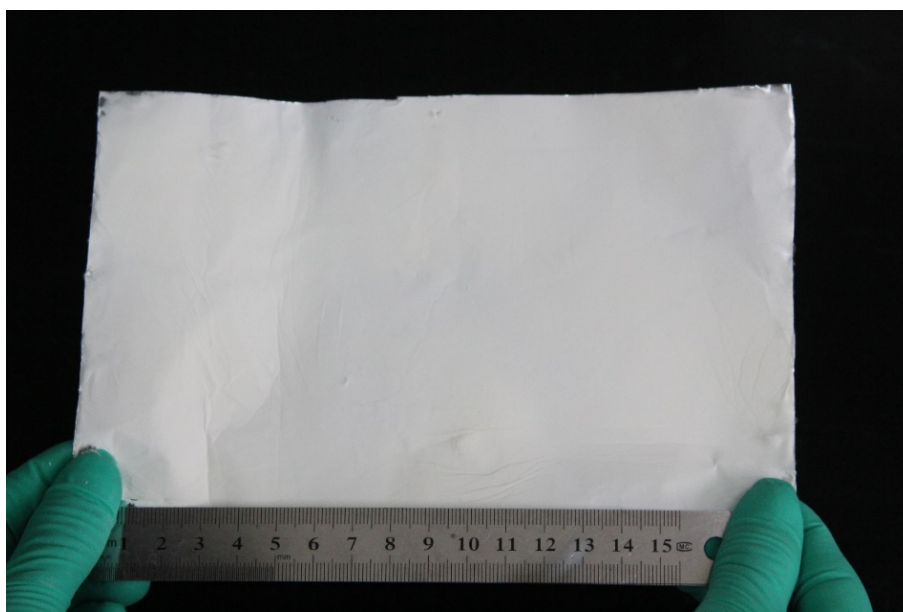


Figure S22. Photo image of nano-BIT-58/PAN based film (70 wt%) in large scale. The large scale cloth was achieved by a position-controlled electrospinning method. A piece of alumina foil (length, 20 cm and width, 14 cm) can be separated into 6 parts. The nozzle of electrospinning device was moved by manual operation every half an hour in a clockwise direction. After 3 h, the full area of the alumina foil is covered with nano-BIT-58/PAN based film (70 wt%) and can be peeled off to be a stand-alone one.

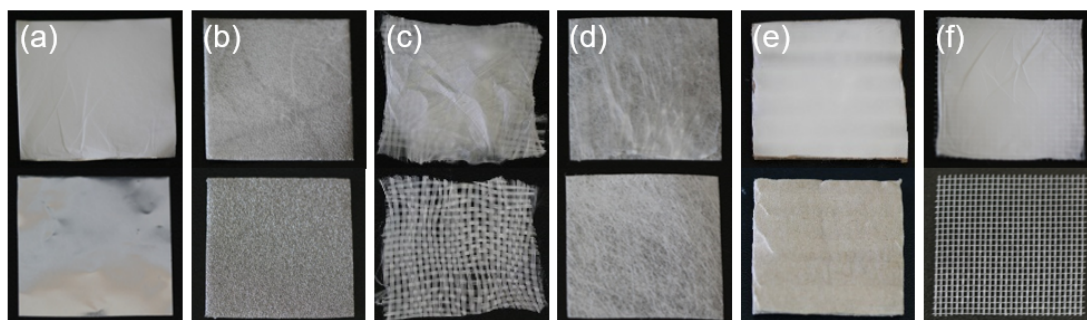


Figure S23. Electrospun coatings on various substrates (size: $4 \times 4 \text{ cm}^2$). a) Aluminum foil. b) Nickel foam. c) Glass cloth. d) Non-woven fabric. e) Cardboard. f) Plastic mesh. Below images are substrates without coatings. All of the coatings were achieved by electrospinning for 30 min with portable electrospinning device.

10. Supplementary information references

- 1 M. J. Cliffe, E. Castillo-Martínez, Y. Wu, J. Lee, A. C. Forse, F. C. N. Firth, P. Z. Moghadam, D. Fairen-Jimenez, M. W. Gaultois, J. A. Hill, O. V. Magdysyuk, B. Slater, A. L. Goodwin and C. P. Grey, *J. Am. Chem. Soc.*, 2017, **139**, 5397-5404.
- 2 J. G. Duan, M. Higuchi, S. Horike, M. L. Foo, K. P. Rao, Y. Inubushi, T. Fukushima and S. Kitagawa, *Adv. Funct. Mater.*, 2013, **23**, 3525-3530.
- 3 M. M. Peng, M. Ganesh, R. Vinodh, M. Palanichamy and H. T. Jang, *Arab. J. Chem.*, doi.org/10.1016/j.arabjc.2014.11.024.
- 4 Z. Wang, C. M. Jin, T. Shao, Y. Z. Li, K. L. Zhang, H. T. Zhang and X. Z. You, *Inorg. Chem. Commun.*, 2002, **5**, 642-648.
- 5 B. L. Chen, Y. Yang, F. Zapata, G. N. Lin, G. D. Qian and E. B. Lobkovsky, *Adv. Mater.*, 2007, **19**, 1693-1696.

6 F. Larachi, J. Pierre, A. Adnot and A. Bernis, *Appl. Surf. Sci.*, 2002, **195**, 236-250.